Materials Science and Engineering A 534 (2012) 693–698

Contents lists available at SciVerse ScienceDirect

Materials Science and Engineering A

journal homepage: www.elsevier.com/locate/msea

Microstructural design for mechanical and electrical properties of spark plasma sintered Al_2O_3–SiC nanocomposites

A. Borrell [a,*], I. Álvarez [a], R. Torrecillas [a], V.G. Rocha [b], A. Fernández [b]

[a] Centro de Investigación en Nanomateriales y Nanotecnología (CINN) (Consejo Superior de Investigaciones Científicas – Universidad de Oviedo – Principado de Asturias), Parque Tecnológico de Asturias, 33428 Llanera (Asturias), Spain
[b] ITMA Materials Technology, Parque Tecnológico de Asturias, 33428 Llanera (Asturias), Spain

ARTICLE INFO

Article history:
Received 6 September 2011
Received in revised form 9 December 2011
Accepted 10 December 2011
Available online 19 December 2011

Keywords:
Sintering
Mechanical characterization
Grain growth
Ceramic composites
Microstructural design

ABSTRACT

Al_2O_3–17 vol.% SiC nanocomposites were prepared by powder mixture of submicrosized α-Al_2O_3, nanosized γ-Al_2O_3 and different nanosized β-SiC. Materials were sintered by spark plasma sintering (SPS) technique at two temperatures (1400–1550 °C) and their electrical conductivity and mechanical properties were investigated. High-density composites have been achieved even at the lowest sintering temperatures and the microstructure characterization shows SiC particles located both within the Al_2O_3 matrix grains and/or at the Al_2O_3 grain boundaries.

It has been demonstrated that microstructure tailoring is possible by suitable selection of starting materials and fast sintering by SPS. Accurate design of nanocomposites microstructures allows obtaining moderately conductive (<100 Ω cm) or insulating (10^8 Ω cm) materials while the chemical composition is similar.

Crown Copyright © 2011 Published by Elsevier B.V. All rights reserved.

1. Introduction

Since the concept of structural ceramic nanocomposites had been proposed by Niihara in 1991 much attention has been focused on their processing routes and mechanical properties improvement [1]. Particularly, Al_2O_3–SiC nanocomposites in which submicrometre or nanometre alumina matrix is reinforced with silicon carbide nanoparticles have been widely studied. In the early 1990s different authors as Nakahira [2], Ohji [3] or Deng [4] revealed that the addition of low percentages of this material (5–17 vol.% of SiC particles) to an alumina matrix produced a large enhancement of the fracture strength and a markedly improved creep resistance on the final composite, compared to pure alumina.

In these materials, the most critical factors that appear to control the properties of use are: positioning of the second phase particles into the matrix (intragranular, intergranular or both), SiC and Al_2O_3 grain size (micrometric or nanometric) and the chemical composition (vol.% of SiC). Deng et al. showed the enhancement of the mechanical properties with a change in the mode of the alumina matrix fracture, from intergranular to transgranular, induced by the dispersion of SiC fine particles into the matrix. Besides the mechanical reinforcement, the electrical properties of composite materials can also be tailored. In particular, alumina based materials reinforced with conductive phases, or semiconductors such as silicon carbide, over the percolation threshold have received special attention. This is due to the advantages that can be offered by electro-conductive ceramics in wide variety fields of applications in industry. It is well known that mathematical calculations fixed a 17% relative volume of conductive phase as percolation threshold when the dispersed phase is formed by spherical particles [5,6].

Al_2O_3–SiC composites are usually sintered by hot pressing (HP) of powder mixtures [7,8]. Although the simultaneous heating and uniaxial pressure applied facilitates the densification of these composites, high temperatures up to 1800 °C are usually required. Due to the high sintering temperatures needed, alumina grain growth and the subsequent final microstructure control is limited. Recently, the spark plasma sintering (SPS) technique allows obtaining full dense materials in a very short time and lower temperatures than conventional sintering techniques [9]. The SPS, also known as field assisted sintering technique (FAST), is a sintering technique widely used in the processing of ceramic materials which can consolidate powder compacts applying an on–off DC electric pulse under uniaxial pressure [10]. This technique can work at heating rates of the order of hundreds degrees per minute combined with the external pressure assistance, reaching high temperatures in a very short time [11,12]. This sintering technique is being profusely applied in the preparation of a wide range of composites, but only three scientific publications can be found dealing with SPS sintered Al_2O_3–SiC materials [13–15]. All of them were focused on the SiC

* Corresponding author. Tel.: +34 985 980 058; fax: +34 985 265 574.
E-mail address: a.borrell@cinn.es (A. Borrell).

0921-5093/$ – see front matter. Crown Copyright © 2011 Published by Elsevier B.V. All rights reserved.
doi:10.1016/j.msea.2011.12.032

particles positioning in the final composite. Nevertheless, there is still no data about the influence that starting materials features and SPS parameters have on the design of these materials microstructure. In particular, raw materials features and processing and/or sintering conditions are especially relevant when the second phase content in the composite is close to the percolation threshold [16].

In the present work, the preparation of different inter/intragranular micro-nanocomposites of Al_2O_3–17 vol.% SiC by spark plasma sintering at relatively low temperatures is proposed. The resulting materials are evaluated in terms of microstructure, electrical conductivity and mechanical properties.

2. Experimental

2.1. Starting materials and mixed powders

The starting materials used in this study were three different commercial Al_2O_3 powders and two silicon carbide powders. Their characteristics have been provided by the suppliers and verified by DRX and TEM, these summarized in Table 1. The commercial alumina Taimei TM-DAR (T) is manufactured by Chemicals Co. Ltd, Japan, alumina Nanotek (N) by Nanophase Technologies Co., USA and alumina Sasol SPA 0.5 (S) by Ceralox Division, USA. These materials have a purity of 99.99%. As a second phase, β-SiC nano-sized powder (Hb) from Hubei Minmetals Corp., China with a purity >98% and β-SiC nano-sized powder (Tp) by Tespint S.A. Belgium with a purity >95% were used.

Powders mixtures containing 17 vol.% of nano-SiC component were prepared by roll milling using ethanol (Panreac Quimica) as solvent in a PET container. High purity (99.5%) alpha alumina balls media of 2 mm diameter were added in a relation to media/powders 4/1. Rotating speed was fixed at 100 r.p.m. and rolling times of 48 h were used to achieve a good dispersion between both phases. After roll milling, the resultant slurry was dried at 60 °C and the dried powder was sieved under 60 μm. The samples were labelled with the capital letters in brackets from each material.

2.2. SPS processing and characterization of sintered bodies

The composite powders mixtures were placed into a graphite die with an inner diameter of 20 mm and cold uniaxially pressed at 30 MPa. Then, they were introduced in a spark plasma sintering apparatus HP D 25/1 (FCT Systeme GmbH, Rauenstein, Germany) under low vacuum (10^{-1} mbar) and sintered at 1400 °C and 1550 °C for 1 min of dwell time and heating rate of 100 °C min^{-1}. Samples were initially pressed at 16 MPa and this load was kept from room temperature up to 600 °C. Then, pressure was increased while heating, reaching 80 MPa within the next 100 °C and being maintained up to the maximum temperature and during dwell time. Real density of the starting powders has been measured by helium picnometry. The obtained values were 3.90 ± 0.2 g cm^{-3} and 3.55 ± 0.2 g cm^{-3} for alpha and gamma alumina powders, respectively, and 3.11 ± 0.1 g cm^{-3} in the case of silicon carbide. The apparent densities of the sintered composites were measured by the Archimedes method using water as medium (ISO-3369) and the real density by He pycnometry. The relative density was calculated as the apparent/real densities ratio.

The samples for hardness and fracture toughness analysis were previously polished (Struers, model RotoPol-31) with diamond to 1 μm roughness. The hardness of the materials was determined using the indentation technique (Buehler, model Micromet 5103) with a conventional diamond pyramid indenter. The diagonals of each indentation were measured using an optical microscope. Thirty diagonals were tested for each composition. Measuring conditions for the Vickers hardness, H_v, were an applying load of 2 N for 10 s and the standard specification ASTM E92-72. To estimate the indentation fracture toughness (K_{IC}), 98 N Vickers indentations were performed on the surface of the samples, inducing Palmqvist cracks, from which the indentation fracture toughness was obtained by method of Niihara [17]. After polishing and thermally etching in vacuum, sintered samples were characterized by field emission scanning electron microscopy (FE-SEM, Zeiss Ultraplus). The electrical resistivity of composite materials was determined according to ASTM C611. The specimens were placed between two sheets of copper connected to a power supply, which allowed working at different current intensities. The measurements were carried out by fixing the intensity of the current at 0.5 A using a multimeter of fixed contacts (9.55 mm separation), determining the voltage drop.

The alumina average grain size of the sintered composites was calculated from the FE-SEM micrographs of the polished and thermally etched surface. For this purpose, the lineal intercept technique for measuring grain size in composites, developed by Wurst and Nelson [18] was used. More than 100 grains were taken into account by this method.

Table 1
Particle size and crystal structure of the powders.

Raw materials	Crystal structure	Mean particle size, d_{50} (nm)
Al_2O_3 (Nanotek)	70(gamma):30(delta)	45
Al_2O_3 (Taimei)	Alpha	150
Al_2O_3 (Sasol)	Alpha	350
SiC (Hubei)	Beta	50
SiC (Tespint)	Beta	80

3. Results and discussion

3.1. Sintering behaviour and mechanical properties

Two temperatures were used for spark plasma sintering tests (1400 °C and 1550 °C). In both cases, nearly fully dense samples (>99.0% relative density) were obtained for all Al_2O_3–17 vol.% SiC composites prepared through the different raw materials combinations tested. In Figs. 1, the microstructures of nanocomposites obtained at 1400 °C and 1550 °C can be observed, where alumina (grey) and silicon carbide (black) can be distinguished and no porosity is observed. When similar composite powder (Al_2O_3–SiC) is sintered by hot-press, it is needed at least 1650 °C and 1 h soaking time [19–21] for total densification, even if the total SiC content is lower (5 vol.%). Then, SPS sintering technique allows attaining total densification of this type of composites in very short processing times and at relatively low temperatures. The strong reduction in processing times is critical if a control of alumina grain growth is desired.

Moreover, the residual porosity was always <0.5% except for NTp at 1400 °C sample that has 0.9% porosity. In this case, the phase transformation of the alumina Nanotek from gamma/delta to alpha during the sintering cycle delays the densification process. If the sintering temperature is increased (1550 °C) the residual porosity is completely removed.

The effect of pressure on sintering has been widely discussed in the literature. The pressure has a mechanical role (higher packing density of particles, rearrangement, breakdown of agglomerates, etc.) as well as an intrinsic role (by increasing the driving force of sintering). Jaafar et al. have reported that the densification of alumina–SiC material by SPS was drastically reduced from 99% to 85% by half reducing the applied pressure from 80 to 40 MPa and maintaining the sintering temperature [13]. Then, the full densification of samples achieved in this work, for both sintering temperatures (1400 °C and 1550 °C) can be favoured by the high

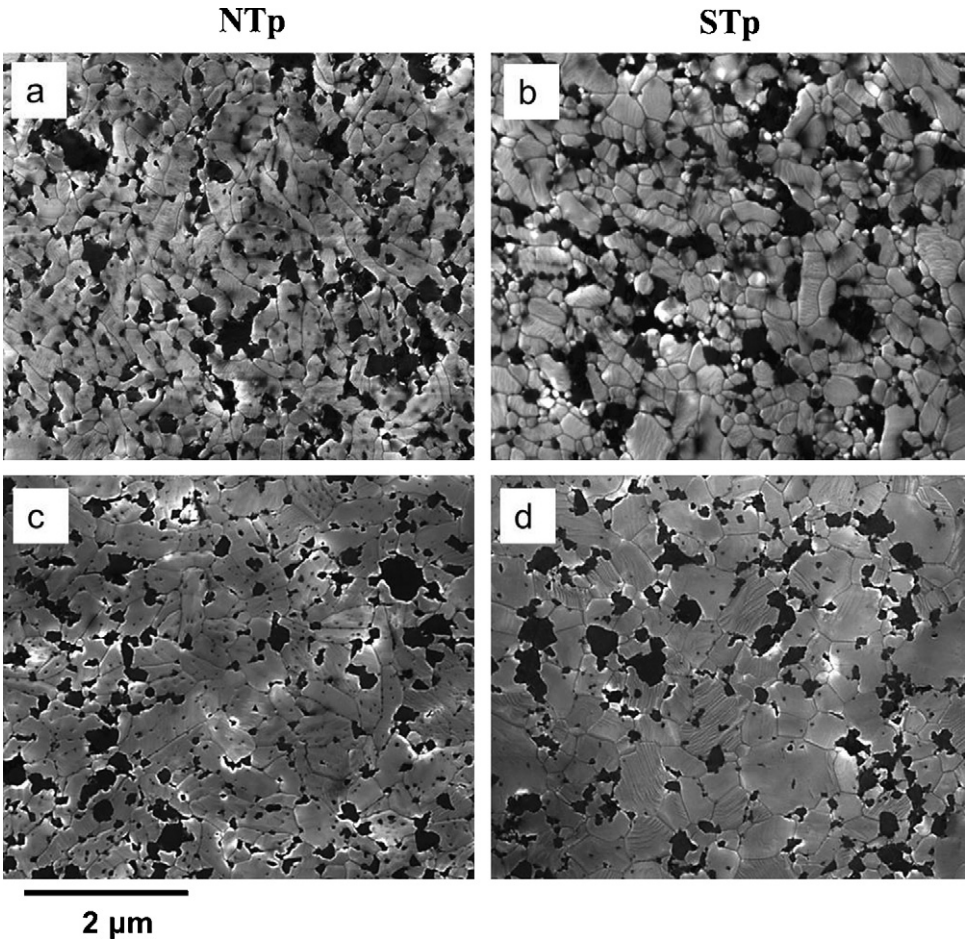

Fig. 1. FE-SEM microstructure of alumina–17 vol.% SiC nanocomposites sintered by SPS at 1400 °C (a) NTp, (b) STp and at 1550 °C (c) NTp, (d) STp.

pressure applied (80 MPa). Despite the final density is similar for both sintering temperatures, differences in the final microstructure are expected, especially when the nanocomposites are prepared by using different raw materials (average size and crystalline phases).

It is known that different diffusion mechanisms operate during the sintering process at high temperature. The high heating rates conventionally used in SPS sintering technique play an important role in the evolution of the material microstructure. High sintering rates such as those used in this work promote lattice diffusion and/or grain boundary diffusion which are major densification mechanisms in the high-temperature regime rather than surface diffusion as a coarsening mechanism [15].

Alumina average grain size, Vickers hardness and fracture toughness measured on specimens sintered by SPS are summarized in Table 2.

Table 2
Grain size, Vickers hardness and fracture toughness of Al_2O_3–17 vol.% SiC nanocomposites sintered by SPS at different temperatures.

Sample	Sintering temperature (°C)	$d_{Al_2O_3}$ (nm)	H_v (GPa)	K_{IC} (MPa m$^{1/2}$)
NTp	1400	430 ± 8	17.9 ± 0.3	3.4 ± 0.1
NTp	1550	590 ± 10	17.8 ± 0.4	4.3 ± 0.1
STp	1400	430 ± 7	19.7 ± 0.4	2.9 ± 0.1
STp	1550	580 ± 10	19.3 ± 0.5	3.3 ± 0.1
TTp	1400	260 ± 6	20.7 ± 0.4	3.1 ± 0.1
TTp	1550	440 ± 8	19.1 ± 0.3	3.2 ± 0.1
THb	1400	170 ± 6	22.0 ± 0.4	5.3 ± 0.1
THb	1550	300 ± 9	21.3 ± 0.5	5.3 ± 0.1

Concerning the hardness values, it can be observed that for all the materials obtained through the different starting materials combinations, the higher hardness values are found at the lower sintering temperature. Two main factors that affect the hardness value of this type of nanocomposites are the density of the material and the grain size of the alumina matrix. Thus, the material defects due to the presence of porosity cause a decrease in its hardness and on the other hand, the Hall–Petch effect predicts a decrease of material hardness with the increase of average grain size for crystalline materials. As it has been previously discussed, total densification of these materials was attained and only in the case of Nanotek based composite obtained at 1400 °C a residual porosity was observed. Moreover, this composite showed the highest alumina grain growth, from 45 nm to 430 nm (SPS test at 1400 °C) or 590 nm (SPS test at 1550 °C). As consequence, Nanotek based composites show the lower hardness values. In the case of alpha alumina starting materials, raw materials with different average grain sizes were selected, that combined with the use of SPS sintering technique allows adjusting the final microstructure features of the composite. When STp and TTp composites are compared, it can be observed how the average grain size of the alumina matrix in the final composite is lower for TTp composites, especially when the sintering temperature was fixed at 1400 °C. If the sintering temperature is increased, the additional alumina grain growth observed in TTp composite cause a decrease of material hardness, being similar to STp composite. Besides the sintering temperature, the presence of SiC particles as second phase also plays an important role in the alumina grain size control. The beneficial effect of the addition of SiC on the refinement of the alumina matrix microstructure has been

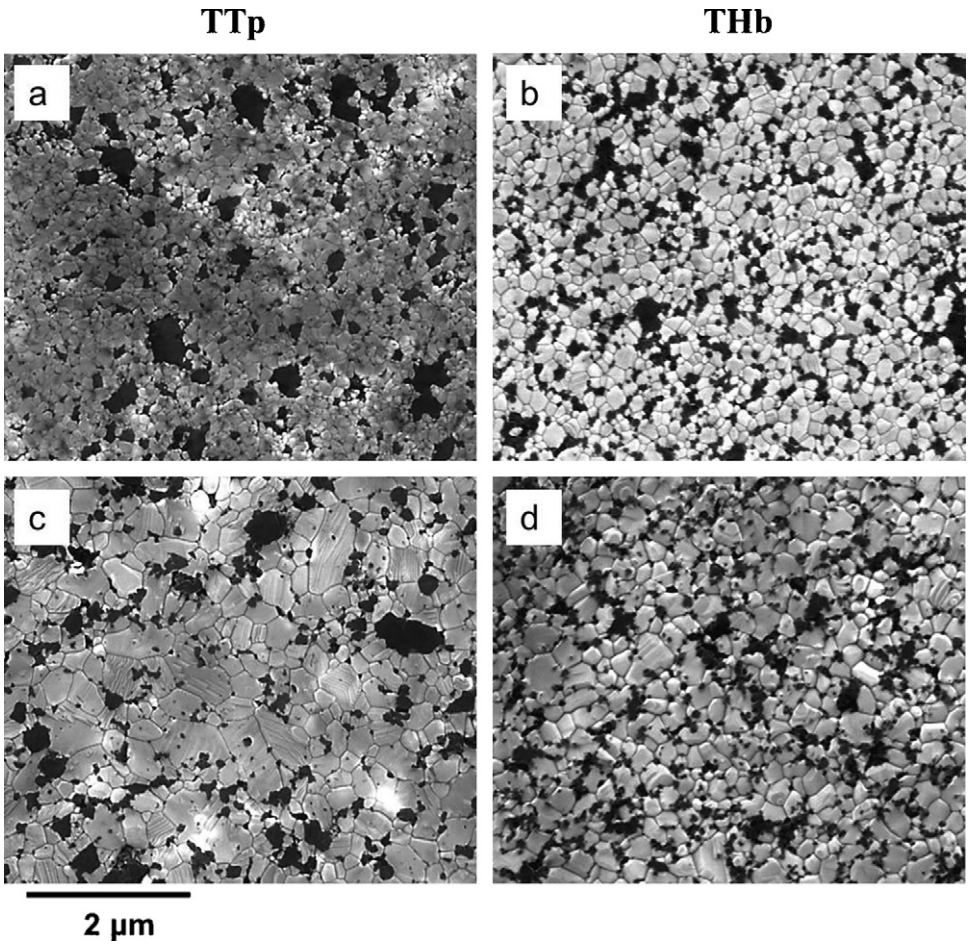

Fig. 2. FE-SEM microstructure of alumina–17 vol.% SiC nanocomposites sintered by SPS at 1400 °C (a) TTp and (b) THb and at 1550 °C (c) TTp and (d) THb.

studied by different authors [15,20,22]. This effect can be clearly observed when TTp and THb materials are compared. As it can be observed in Fig. 2, the particles of SiC are more homogeneously dispersed in the alumina matrix in THb material and therefore, they hinder the alumina grain growth more efficiently. Thus, the average grain size of alumina matrix in THb composite obtained at 1400 °C is 170 nm, very close to the starting powder size (150 nm). The combination of low sintering temperature allowed by SPS sintering technique and the grain growth blocking effect due to the fine distribution of SiC particles leads to a dense nanocomposite with grain size phase components similar to the corresponding starting powders. The hardness of the resulting nanocomposite is the highest of the samples sintered (22.0 GPa). The suitable dispersion of SiC nanoparticles also causes an efficient grain growth inhibition at high temperature. Thus, the alumina average grain size of THb material obtained at 1550 °C is similar to TTp prepared at 1400 °C.

3.2. Fine microstructure and electrical conductivity

In Fig. 3, the high magnification FE-SEM and fracture surface micrographs of TTp and THb Al_2O_3–17 vol.% SiC nanocomposites sintered by SPS at 1550 °C are shown. Fracture toughness (K_{IC}) values of the composites prepared, are usually in the 2.9–4.3 MPa $m^{1/2}$ range. Traditional reinforcement mechanisms such as crack bridging are limited due to the small grain size observed in the nanocomposites. However, the values of fracture toughness of THb composites are noticeably high. In this case, the efficient dispersion of SiC nanoparticles in the alumina matrix promotes alternative mechanisms such as crack deviation or residual stresses leading to relatively high fracture toughness in these composites. The nature of alumina grains fracture is mainly transgranular in both cases. The presence of SiC grains can be considered as the crack deflection sites for crack growth. When the alumina grain size is higher (TTp), the number of the crack deflection sites is reduced and the crack growth rate increases. Moreover, transgranular fracture is also observed for SiC grains with grain size >100–200 nm as those observed in TTp sample. Then, crack propagation is facilitated and fracture toughness is rather average. On the other hand, the dispersion of SiC nanoparticles in THb sample increases the number of the crack deflection sites noticeably. As the size of SiC nanoparticles is very small, no transgranular fracture of SiC phase is observed. Then, crack propagation is hindered and fractures toughness is improved.

The nanocomposites studied in this work are composed by a dielectric matrix (alumina) and a semiconductor with second phase (silicon carbide) which can provide a path to electrical conduction if it is well distributed [23]. Then, the mechanism of electrical conduction for Al_2O_3–SiC nanocomposite materials is the formation of a continuous network of SiC particles within the Al_2O_3 matrix. The distribution of SiC nano-particles will be one of the most important parameters for obtaining electro-conductive materials [24]. Moreover, the position of SiC nanoparticles will be influenced by alumina matrix evolution. The growing of alumina grain size from the starting powder to dense material can favour an increase of the relative content of SiC nanoparticles in intragranular position. An alumina growing factor (AGF) was calculated as $AGF = (d_{final} - d_0)/d_0$ where d_{final} and d_0 are the alumina average grain size in the sintered material and starting powder respectively. On the other hand, the percentage SiC nanoparticles at inter/intragranular positions was calculated through image analysis. These parameters are

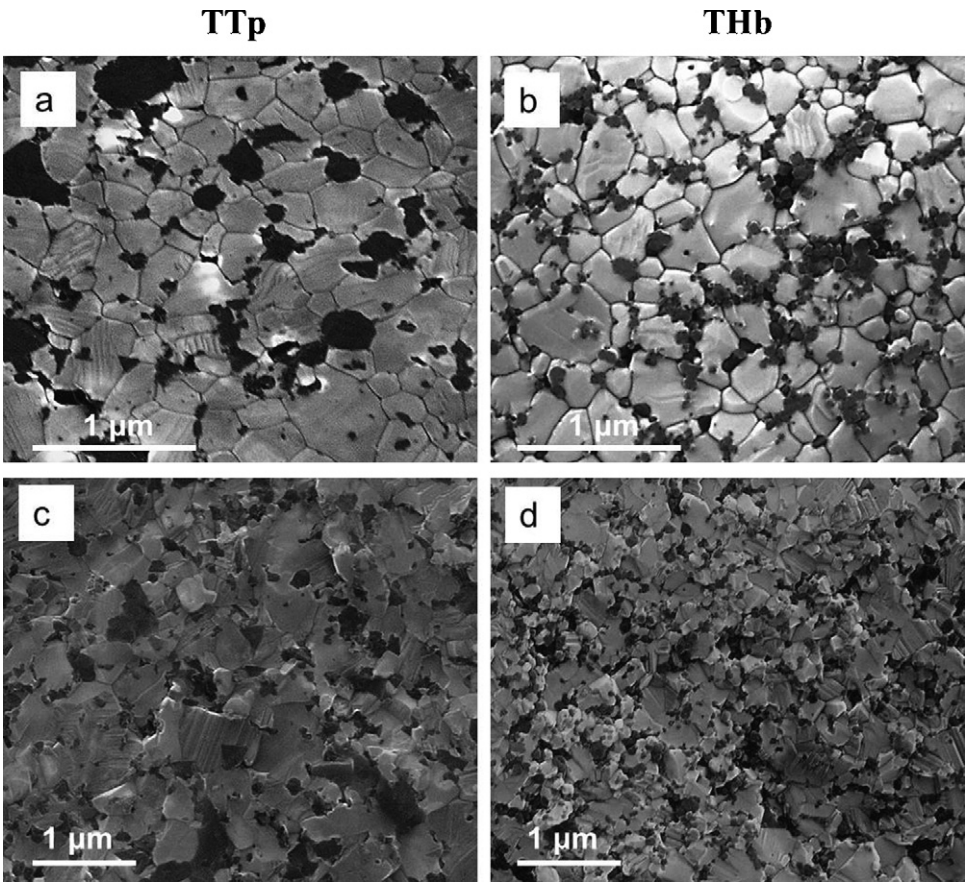

Fig. 3. FE-SEM micrographs of alumina–17 vol.% SiC nanocomposites sintered by SPS at 1550 °C: microstructure (a) TTp, (b) THb and fracture surface (c) TTp, (d) THb.

summarized in Table 3 where the electrical resistivity values of the resulting composites are also included.

Considering that nanocomposites are prepared by a powder mixing process, 100% of SiC particles are placed at intergranular positions in the initial state. They can only progress to intragranular positions when they are trapped by alumina grains during their growth. As it could be expected, AGF and relative content of SiC particles at intragranular positions (reduction of % SiC inter) increase with the sintering temperature. However, the evolution of these parameters is clearly influenced by the type of alumina starting powder. It is remarkable the AGF, and therefore, the % SiC intragranular for composites prepared using Nanotek alumina powder (NTp). The increase in size from 45 nm to 430 nm or 590 nm favours the entrapment of SiC particles leading to a noticeable % SiC intra (>25%). The great alumina grain growth for Nanotek powder is related with phase transformation as it can be concluded when it is compared with TTp composites, where the same SiC powder content and type is used with an alternative small size alpha alumina (Taimei, 150 nm). It is also observed that this transformation causes abnormal grain growth of the alumina particles during sintering. Moreover, the entrapment of SiC particles mainly occurs during the densification process (that includes the phase transition) and it is negligible during the further grain growth. Thus, when the material is sintered at 1400 °C, 99.1% r.d. is achieved and 25.7% of SiC content is placed at intragranular positions. The increase of sintering temperature up to 1550 °C promotes an additional grain growth (from 430 to 590 nm) but the SiC content at intragranular positions remains constant (26.2%). It is well known that heating over the temperature needed for achieving material densification favours grain growth. Although additional SiC particles entrapment could be expected, the reduction of effective SiC content at grain boundaries, from 17 vol.% to 12.6 vol.%, due to the evolution of 25% of SiC content from inter to intragranular position facilitates alumina grain growth through SiC free areas as it can be clearly observed in the FE-SEM micrograph Fig. 1a and c.

Concerning STp, TTp and THb materials, silicon carbide nanoparticles remain at intergranular position when the samples are sintered at 1400 °C while an increase of the sintering temperature up to 1550 °C leads to different relative percentages of SiC particles at intragranular position, being 13.0, 5.4 and 1.8% for TTp, STp and THb, respectively. TTp sample shows the highest AGF, excluding NTp composites, and this microstructure evolution facilitates the entrapment of SiC particles. The influence of SiC distribution can be observed if this sample is compared with THb composites. In that case, the efficient distribution of SiC nanoparticles within the whole alumina matrix, drastically reduce the (Taimei) alumina

Table 3
Microstructure parameters and electrical resistivity of Al_2O_3–SiC nanocomposites sintered at different temperatures.

Sample	Sintering temperature (°C)	AGF	% SiC inter	Resistivity (Ω cm)
NTp	1400	8.55	74.3 ± 0.3	$5.80 \times 10^2 \pm 0.05$
NTp	1550	12.11	73.8 ± 0.4	$1.50 \times 10^3 \pm 0.05$
STp	1400	0.23	99.9 ± 0.4	$3.10 \times 10^1 \pm 0.05$
STp	1550	0.66	94.6 ± 0.4	$1.70 \times 10^2 \pm 0.05$
TTp	1400	0.73	99.8 ± 0.5	$2.40 \times 10^2 \pm 0.05$
TTp	1550	1.93	87.0 ± 0.4	$3.00 \times 10^3 \pm 0.05$
THb	1400	0.13	99.6 ± 0.3	$3.60 \times 10^8 \pm 0.05$
THb	1550	1.00	98.2 ± 0.4	$2.56 \times 10^7 \pm 0.05$

grain growth and very low percentage of SiC particles pass from inter to intragranular position. Finally, it is interesting to remark that, even if the average alumina grain size of NTp and STp are similar for composites prepared at both sintering temperatures, the SiC particles distribution is noticeably different due to microstructure evolution. Then, once it is known the starting powders evolution with temperature, the choice of raw materials can be used as an additional tool for fine microstructure design.

The electrical conductivity of composite materials formed by dielectric and conductive or semiconductor components strongly depends on their microstructures, especially when the content in conductive phase is close to percolation threshold. From the technological point of view, a value of electrical resistivity <100 Ω cm is particularly useful for ceramics. This is considered the limit of resistivity for applying electrodischarge machining (EDM), enabling the fabrication of complex shape ceramic components by a simple and economic method [25].

The composites sintered at both temperatures (1400 °C and 1550 °C) can be ordered according to their electrical resistivity as follows: THb ≫ NTp ∼ TTp > STp. Taking into account that the growth of the SiC particles is negligible during the sintering process, the electrical conductivity will be related with the possibility of forming a continuous network of SiC particles within the Al_2O_3 matrix. Two factors will affect the formation of that continuous network. Firstly, the alumina grain size will establish the available grain boundaries to be covered by SiC particles and the % SiC inter will limit the silicon carbide nanoparticles that are contributing to form the network.

STp composites are prepared using the alumina starting powder with the biggest average grain size. Then, the available grain boundaries for locating SiC particles is limited which combined with their low AGF, and therefore high % SiC inter, allow obtaining composite materials with the lowest electrical resistivity. Although alumina grain size of NTp composites is similar to STp, the reduction in % SiC inter is the responsible of electrical resistivity increase. TTp has lower alumina grain size than STp and NTp composites and therefore the available grain boundaries for locating SiC particles are relatively high. The resulting increase in the interspace between SiC nano-particles hindered the formation of an interconnecting current path in the sample and caused the degradation of electrical conductivity. An extreme case of this effect can be observed in THb composites. The efficient hindering of alumina grain growth combined with the homogeneous distribution of SiC nanoparticles reduces significantly the number of SiC-SiC particles contacts and the obtained material is completely dielectric.

Then, the considerable change in electrical properties with sintering temperature and starting materials can be understood in terms of a strong correlation between the microstructure and electrical conductivity.

It is important to remark the change of electrical resistivity value for STp composites obtained at 1400 °C and 1550 °C. The composite sintered at lower temperature has an electrical resistivity of 31 Ω cm (<100 Ω cm) whereas that corresponding to the material obtained at 1550 °C is 170 Ω cm (>100 Ω cm). Although this difference has been previously discussed in terms of microstructure features, it is interesting to highlight the opportunity offered by spark plasma sintering technique as a tool for microstructural designing. This technique allows obtaining dense material at low temperature, hindering further grain growth that can lead to modified mechanical or electrical properties.

4. Conclusions

The influence of starting materials (α-Al_2O_3, γ-Al_2O_3 and β-SiC) average grain size and sintering parameters on the microstructure of the dense materials obtained was studied. It has been proved how mechanical and electrical properties of Al_2O_3–SiC composites can be influenced by fine control of micro/nanostructure of the material. The short processing times required by spark plasma sintering technique facilitates the preparation of dense composite materials with average grain size close to the starting materials used. The improvement in the hardness and fracture toughness of Al_2O_3–SiC nanocomposites was related to the densification behaviour and microstructural evolution, as well as the effect of the fine SiC distribution. Al_2O_3–SiC nanocomposite prepared by α-Al_2O_3 submicrosized, STp, sintered at 1400 °C showed the highest electrical conductivity. Intergranular/intragranular positioning of SiC nanoparticles and matrix grain size affect the interconnection degree of SiC component required for electrical conductivity. Material with similar composition but prepared with different starting powders and sintering conditions shows electrical resistivity values even six orders higher.

Acknowledgements

Financial support of this work by the European Commission is gratefully acknowledged (IP Nanoker P3-CT-2005-515784). A. Borrell acknowledges the Spanish Ministry of Science and Innovation for Ph.D. grant (MAT2006-01783).

References

[1] K. Niihara, J. Ceram. Soc. Jpn. 99 (1991) 974–982.
[2] K. Niihara, A. Nakahira, T. Uchiyama, T. Hirai, in: R.C. Bradt, A.G. Evans, D.P.H. Hasselman, F.F. Lange (Eds.), Fracture Mechanics of Ceramics 7, Composites, Impact, Statistics, and High-temperature Phenomena, Plenum Press, New York, 1986, pp. 113–116.
[3] T. Ohji, T. Hirano, A. Nakahira, K. Niihara, J. Am. Ceram. Soc. 79 (1996) 33–45.
[4] Z.Y. Deng, J.L. Shi, Y.F. Zhang, T.R. Lai, J.K. Guo, J. Am. Ceram. Soc. 82 (1999) 944–952.
[5] D. Stauffer, A. Aharony, Introduction to Percolation Theory, T.F., London, 1992.
[6] D.S. McLachlan, M. Blaszkiewicz, R.E. Newnham, J. Am. Ceram. Soc. 73 (1990) 2187–2203.
[7] Y.M. Ko, W.T. Kwon, Y.W. Kim, Ceram. Int. 30 (2004) 2081–2086.
[8] X. Sun, J.G. Li, S. Guo, Z. Xiu, K. Duan, X.Z. Hu, J. Am. Ceram. Soc. 88 (2005) 1536–1543.
[9] M. Omori, Mater. Sci. Eng. A 287 (2000) 183–188.
[10] R.G. Joanna, Z. Antonios, Mater. Sci. Eng. A 287 (2000) 171–177.
[11] Y. Wang, Z. Fu, Mater. Sci. Eng. B 90 (2002) 34–37.
[12] Z.A. Munir, U. Amselmi-Tamburini, M. Ohyanagi, J. Mater. Sci. 41 (2006) 763–777.
[13] M. Jaafar, G. Bonnefont, G. Fantozzi, H. Reveron, Mater. Chem. Phys. 124 (2010) 377–379.
[14] L. Gao, H.Z. Wang, J.S. Hong, H. Miyamoto, K. Miyamoto, Y. Nishikawa, S.D.D.L. Torre, J. Eur. Ceram. Soc. 19 (1999) 609–613.
[15] J.H. Chae, K.H. Kim, Y.H. Choa, J. Matsushita, J.W. Yoon, K.B. Shim, J. Alloys Compd. 413 (2006) 259–264.
[16] H.K. Janssen, U.C. Täuber, Ann. Phys. (2005) 147–192.
[17] K. Niihara, J. Mater. Sci. Lett. 2 (1983) 221–223.
[18] J.C. Wurst, J.A. Nelson, J. Am. Ceram. Soc. 55 (1972) 109–111.
[19] H.Z. Wang, L. Gao, L.H. Gui, J.K. Guo, Nanostruct. Mater. 6 (1998) 947–953.
[20] Y. Xu, A. Zangvil, A. Kerber, J. Eur. Ceram. Soc. 17 (1997) 921–928.
[21] H.Z. Wang, L. Gao, J.K. Guo, Ceram. Int. 26 (2000) 391–396.
[22] B. Baron, C.S. Kumar, G.L. Gonidec, S. Hampshire, J. Eur. Ceram. Soc. 22 (2002) 1543–1552.
[23] K. Irmscher, Mater. Sci. Eng. B 91–92 (2002) 358–366.
[24] F. Lux, J. Mater. Sci. 28 (1993) 285–301.
[25] K.H. Ho, S.T. Newman, Int. J. Mach. Tools Manuf. 43 (2003) 1287–1300.